Applied Physics A (2023) 129:408
https://doi.org/10.1007/s00339-023-06629-7

Applied Physics A
Materials Science & Processing

Influence of cracks on fracture strength and electric power losses in Silicon solar cells at high temperatures: deep machine learning and molecular dynamics approach

S. D. V. S. S. Varma Siruvuri[1] · P. R. Budarapu[1] · M. Paggi[2]

Received: 14 February 2023 / Accepted: 1 April 2023 / Published online: 10 May 2023

Abstract
Significant electric power losses in the presence of micro-cracks in Silicon-based photovoltaic solar cells have been reported in the literature. In this study, the fracture strength and the loss in electric power of Silicon-based solar cells are investigated considering the influence of crack size, orientation, type and temperature. Deep machine learning models are developed to estimate the fracture strength and the electric power of Silicon-based solar cells with initial cracks. The developed networks are trained with the help of data generated from molecular dynamics simulations. Therefore, molecular dynamics simulations are performed by considering initial edge/center cracks for ten different sizes, four different orientations, and operating at six different temperatures. Later on, results from molecular dynamics simulations are used to train and test the developed deep machine learning models. Results are validated by comparing them with the molecular dynamics simulation results, where a good agreement is observed. Thus, the proposed deep machine learning models can serve as tools to quickly estimate the fracture strength and electric power of Silicon-based solar cells containing initial cracks of arbitrary size, orientation, and operating temperatures.

Keywords Photovoltaic Silicon solar cells · Micro-cracks · High temperatures · Fracture strength · Electric power · Deep machine learning · Molecular dynamics simulations

1 Introduction

Microcracks are bound to generate in solar cells based on Silicon due to various reasons [1] and influence their performance [2, 3]. A program to predict the nature and source of flaws and hence, the mechanical strength of cells is provided in [4]. Based on the studies in [5] the size, position, and orientation of the micro-cracks are found to influence the electric power output produced. The authors in [6] demonstrated the influence of micro-cracks on the carrier lifetime. They reported that the micro-cracks can serve as recombination centers leading to performance degradation of solar modules. In [7], the authors reported that the orientation of cracks had a significant impact on the PV module performance. This means, all cracks do not tend to decrease the electrical power output in Silicon solar cells of the same amount [8, 9]. The cracks parallel to the bus-bars were found to be critical due to increase in the electrically insulated cell area. A particular combination of cracks which tend to open and propagate with the application of mechanical loads, finally leading to the formation of isolated areas and hence decrease in electrical power output were investigated in [10]. The distribution of mechanical strength of Silicon-based photovoltaic (PV) solar cells with micro-cracks is predicted with a model which is described in [11]. A statistical fracture stress distribution of Silicon PV wafers is discussed in [12].

The fracture performance of solar cells in a given module subjected to combined thermal and mechanical loads is studied in [13]. Behavior of fracture strength and the Young's modulus of photovoltaic cells at room temperature is studied in [14]. The room temperature fracture strength of Silicon solar cell was found to reduce by half when it is subjected to thermal cycling [15]. Thermal loads in combination with mechanical, electrical, and chemical loads can influence the

✉ P. R. Budarapu
pattabhi@iitbbs.ac

[1] School of Mechanical Sciences, Indian Institute of Technology, Bhubaneswar 752050, India

[2] IMT School for Advanced Studies Lucca, Piazza San Francesco 19, 55100 Lucca, Italy

performance of the solar module [16, 17]. On the other hand, with an increase in the annealing temperature in oxygen, the fracture strength of Silicon was observed to be significantly increased [18].

The relationship between Silicon wafer surface roughness and mechanical strength was examined in [19] and the authors reported that the fracture strength of Silicon wafers increased with decreasing size of the pyramids in the surface textures. Finite-element modeling and digital image correlation techniques were explored to investigate the mechanical stability of Silicon solar cells in [20], where the authors concluded that the strength of crystalline Silicon cell significantly increased with the removal of the saw damage. The degradation of fracture strength was studied with a decrease in temperature, up to -40°C in [21] and the regions next to the interconnect wires were reported to undergo high stresses, apart from the out-of-plane shear stresses exceeding the shear strength of Silicon, leading to nucleation of microcracks. To understand the dynamic fracture response of single-crystalline Silicon solar cells subjected to cyclic stress, an experimental examination is conducted in [22].

Estimation of fracture properties of Silicon using quantum mechanics (QM) and molecular dynamics (MD)-based simulations gained advantage to overcome the challenges experienced during experimental studies. The mechanical performances of Silicon wafers in three different orientations considering point defect was investigated through molecular dynamics simulations in [23], where an exponential reduction in yield strength and the release elastic strain energy was reported. The mechanical properties of kinked Silicon nanowires in the presence of defects were studied using molecular dynamics simulations [24]. In [25], the mechanical stress along with the fracture behavior of cracked Silicon PV module is characterized using techniques based on synchrotron X-ray diffraction. The electric-field-induced second harmonic generation of phenylpolyenes in chloroform solution is estimated using density-functional theory in [26]. The influence of temperature (up to 1273 K) on fracture properties of single crystal Silicon depending on various crystallographic orientations was reported in [27].

On the other hand, a direct solution of any specific problem involving mathematical–physical description poses several challenges due to the involved complexities. Therefore, approaches using machine learning-based models have evolved more recently as intelligent tools for providing quick solutions to problems involving recurring experiences [28]. For instance, the stress and strain curves of composite structures can be predicted using a convolution neural network as in [29]. The crack propagation can also be predicted using a long short term memory [30]. Crack size can be predicted using Jaya optimization clubbed with an artificial neural network as in [31]. A general two-stage deep learning framework made of separated training of two pipe-lined predictive models to perform the generalization with reduced computational expenses is proposed in [32]. A neural network-based decoupled computational homogenization method for nonlinear elastic materials is introduced in [33]. Different types of rail profiles are recognized using a deep convolutional neural network in [34]. A variety of fracture problems were solved using various deep machine learning (DML) models that were proposed in recent times [35].

To the best of authors' knowledge, estimation of electric power and the fracture strength of Silicon photovoltaic solar cell as a function of thermo-mechanical loads, considering the initial cracks of different sizes, types, and oriented at different angles with the externally applied mechanical load using the combined machine learning and molecular dynamics approaches is yet to be reported. In the current study, models are developed using deep machine learning to quickly estimate the fracture strength and the electric power of Silicon solar cell. The novelties in the study presented here are: (i) developing the deep machine learning models to estimate the electric power and fracture strength of Silicon wafers, (ii) establishment of correlation between the effective area available for power production and the corresponding electric power output, and (iii) carrying out performance analysis to study the influence of the aforementioned parameters on the power output and the fracture strength of Silicon solar cell.

The upcoming paragraphs in the article are organized as follows. Section 2 is dedicated to discuss the approaches involving molecular dynamics to estimate the electric power at the fracture along with the fracture strength of Silicon-based solar cell. Furthermore, the architecture along with the performance of the proposed DML model are included. Section 3 is dedicated to investigate the performance of Silicon solar cell subjected to thermo-mechanical loads. Furthermore, parametric studies and validation of the results of the developed two models are discussed. The main findings are emphasized in Sect. 4.

2 Modeling aspects

2.1 Molecular dynamics model

In this section, an investigation using the molecular dynamics studies is carried out to estimate the power output and fracture strength characteristics of PV Silicon-based solar cells considering the effect of initial crack and operating temperatures. A domain made of Silicon with pre-existing edge and center cracks is considered for the simulations, see the schematic Fig. 1. Both the cracks are placed at the mid-height of the domain. Furthermore, the fracture strength and power output are estimated as a function of crack size and its orientation at different temperatures.

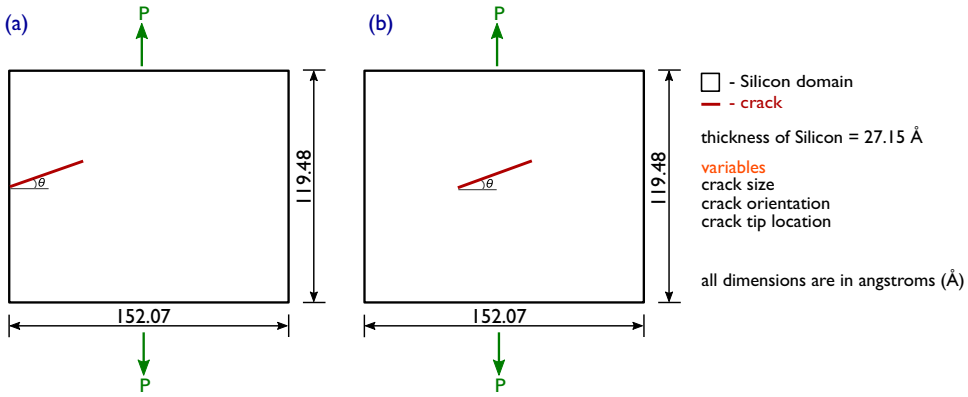

Fig. 1 Schematics of simulation domains, considering an initial (**a**) edge and (**b**) center cracks, subjected to uni-axial tensile load

Therefore, an initial crack of different sizes in the following proportionate ratios of width of the domain(w): 2.5%, 5%, 10%, 20%, 30%, 40%, 50%, 60%, 70%, and 80%, and four different orientations: 0°, 30°, 45° and 60° are considered for the analysis. Estimates of the fracture strength are made in relation to temperature considering six temperatures: 0 K, 300 K, 323 K, 353 K, 600 K, and 900 K. Since the typical operating temperatures of solar cells are not more than 353 K, the power output is estimated at the first four temperatures mentioned above. The group of atoms on the domain's top and bottom regions are subjected to displacement loads to study the deformation characteristics. The power output characteristics as the domain deforms are estimated as follows:

$$P = \frac{PE_f - PE_0}{t} \tag{1}$$

where `P` is the electric power output, PE_f is the total potential energy at the time t of the first bond break and PE_0 is the initial total potential energy of the system.

In the present study, the Silicon domain is prescribed with a strain rate of $\approx 1\ ps^{-1}$, by setting the velocities of the boundary atoms. Domains of various sizes varying between 97.74Å×48.87Å×21.72 Å and 173.76Å×152.04Å×43.44Å are considered for convergence tests. When the above pristine domains are subjected to the same strain rate of $1\ ps^{-1}$, the fracture strength is found to converge to ≈19 GPa for domains of sizes greater than or equal to 152.04Å×119.46Å×32.58Å, at 0 K. Therefore, a domain of size of 152.04Å×119.46Å×32.58Å and a strain rate of $1\ ps^{-1}$ are adopted for all simulations. The selected domain size corresponds to 28, 22, and 5 unit cells in [100], [010], and [001] crystallographic directions, respectively. The Silicon domain's fracture strength is estimated as the stress at the instant of first bond break. The charges are estimated with the help of energy minimization in LAMMPS. Initially zero charge is set on the Silicon atoms. Later on, using charge-optimized many-body (COMB) potential function [36, 37] charge equilibration is performed to estimate the charge on individual atoms. With an electronegativity precision of 0.0001, the charge equilibration is performed after every 100 time-steps. The interactions between the Silicon atoms is simulated using `ffield.comb` potential function. Furthermore, using the pair style `comb` as a variable charge potential and based on the equalization of electronegativity, the variable charge-second generation COMB potential [37] is evaluated.

2.2 Deep machine learning

An artificial neural network (ANN)-based computational model comprises of three interconnected layers of neurons, namely: input, hidden, and output layers. Deep neural networks (DNN) are the neural networks with two or more hidden layers. In deep machine learning, the connections between the neurons can be altered through various learning methods. The non-linearity to the network is introduced through activation functions. In addition, they aid in limiting neuron output such that diverging neurons do not lead to paralyzing the neural network. Linear activation functions [38] and Rectified Linear Unit (ReLU) are considered in the present study to develop the networks.

The network's weights and corresponding biases are initially set at random. Moreover, with the help of error back propagation method, they are changed in an iterative fashion until the total error is minimized. In the current study, Adam optimizer [39], a computationally efficient optimization algorithm is adopted. The optimized weights and biases are evaluated by minimizing the mean squared error (MSE) loss function. This loss function is employed to assess how well the DNN model is trained. The Python [40] language combined with Keras API [41] are used to develop the DNN model. Hidden layers are varied to measure their performance and construct the neural networks sequentially. The number of neurons are maintained constant while varying the number of hidden layers until the network parameters

are optimum. Thus, the obtained neural networks are further tested for the robustness. The network's efficiency is assessed with the help of R^2 score on the test data and the MSE loss function.

2.2.1 DML model for fracture strength and power output

The architecture and number of layers of the developed DNNs for estimating the fracture strength and generated electric power from the Silicon domain discussed in Sect. 2.1, are shown in Figs. 2 and 3, respectively. According to Fig. 2, to estimate the fracture strength of Silicon, the second, third, fourth, and fifth layers are shared with 32, 16, 8, and 2 number of neurons, respectively. On the other hand, as shown in Fig. 3, the hidden layers in the DNN to estimate power generation are distributed as follows: second layer-64, third layer-32, fourth layer-32, fifth layer-16, sixth layer-8, and seventh layer-2 neurons. Molecular dynamics simulation results are used to build a data set for training the developed DNN. The number of data points available for electric power are lesser as compared to the number of data points for fracture strength. Therefore, there are more hidden layers in the DNN used to estimate the electric power than that of the DNN used for the estimation of the fracture strength.

In total, 402 and 268 data samples are produced using MD simulations to estimate the fracture strength and electric power, respectively. The data set is generated considering the preliminary crack orientated at 0° for edge, center cracks with varying size and orientation of crack along with the domain temperature. The training, testing, and validation sets are divided up into the data set at random. The test data set, which makes up 20% of the overall data set is hidden during training and used to assess performance of the DML model. The train data set is randomly divided into the validation data set at a 90:10 ratio. The neural network can understand the characteristics from the sample data by fitting the sample set that is trained. In order to avoid the model from over fitting, the validation data set aids in setting the hyper parameters during training by providing an objective evaluation of model fit on the sample data set used for training the network.

The effects of hyper parameters, such as: batch size, number of epochs, learning rate, number of hidden layers and corresponding neurons, optimization algorithms, and activation functions are studied before selecting their values. To begin with, a batch size of one is considered, where the developed model is observed to be specific to the training set and the training and testing losses are small. Furthermore, the influence of batch size is tested with double the batch size in subsequent cycles. With a batch size of four, the losses during training and testing are found to be still smaller and the model is ready to be tested on an arbitrary system. Thus, a batch size of four is selected in the present study, without loss in performance and considerably reduced computational cost as compared to the network with a batch size of one. To help the model learn and comprehend the issue, all the parameters are scaled separately from 0 to 1 using the min–max method.

Both the extreme network layers employ a linear activation function, whereas, all other layers use a ReLU function. The model is trained using the Adam optimizer [39] and MSE loss function. The network has received training on an

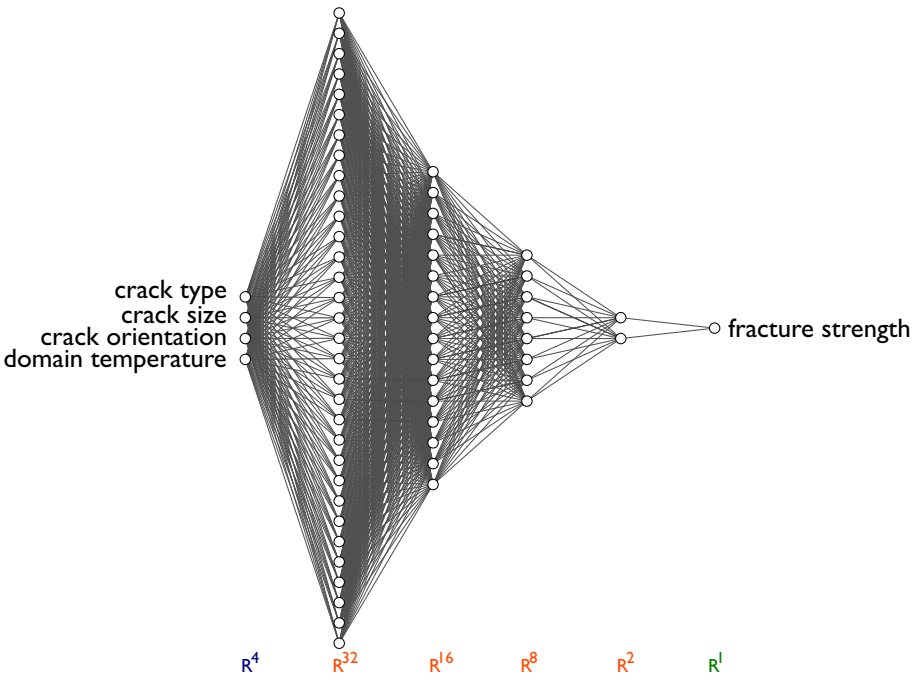

Fig. 2 Architecture and number of layers of the developed DNN for predicting the fracture strength of Silicon

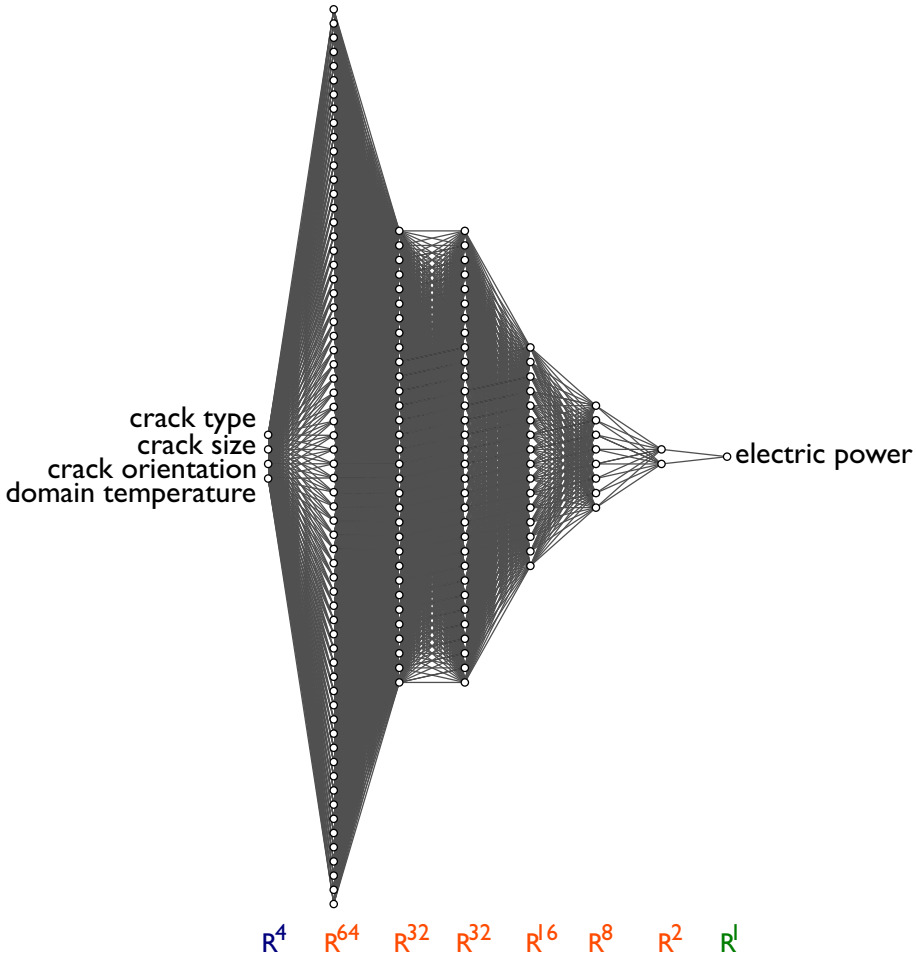

Fig. 3 Architecture and number of layers of the developed DNN for estimating the generated electric power from the Silicon domain

NVIDIA Corporation TU104GL Quadro RTX 4000 graphic card. The network is trained for 500, 1000 epochs with a specified learning of 0.001 for 100, 200 epochs, 0.0001 in the next 200, 400, proceeded by 0.00001 for the following 200, 400 epochs for fracture strength and electric power, respectively. Therefore, the network is gradually trained for reduced error tolerance. This ensures the improved learning curve and hence, the robustness.

The proposed DNN is trained using estimates of Silicon fracture strength obtained from MD simulations by altering various parameters. A total of 402 and 268 data sets, respectively, containing the fracture strength and electric power information, where 322 and 214 sample sets are employed for training and validation, and the testing is performed with 80 and 54 data samples. The developed DNN is trained for 500, 1000 epochs, for fracture strength and electric power, respectively. The loss in relation to epochs for fracture strength and power output are shown in Fig. 4a, b, respectively.

In Fig. 4, the training loss is found to be drastically decreased during the course of first 10 epochs. This indicates that within the first 10 epochs, the model can locate a better local minimum. A comparison of training as well as validation losses in relation to the epochs number is also shown in Fig. 4. The model is observed to be not over predicting on the sample set used for training, as shown by the comparable declining trend in the losses for training and validation. In addition, the close-ups of Fig. 4a, b show that the peaks in learning and validation losses are found to take place at the relevant epochs, further supporting a excellent fit. At the end of the training process, the train and test losses are, respectively, found to be 0.000458 and 0.000458, for fracture strength and 0.000104 and 0.000104 for electric power. On the other hand, a loss of 0.001025 and 0.000953 is observed for fracture strength and electric power, respectively. To choose the best performance, a random sampling is run ten times.

An R^2 score of 0.9737 and 0.9851 is found while training the fracture strength and electric power networks, respectively. Test data set, signifying the variance in respective parameters is explained considering dimension and positioning of the crack along with the domain temperature. The effectiveness of the developed network for test and train data sets is shown in Fig. 5. The fracture strength of Silicon is

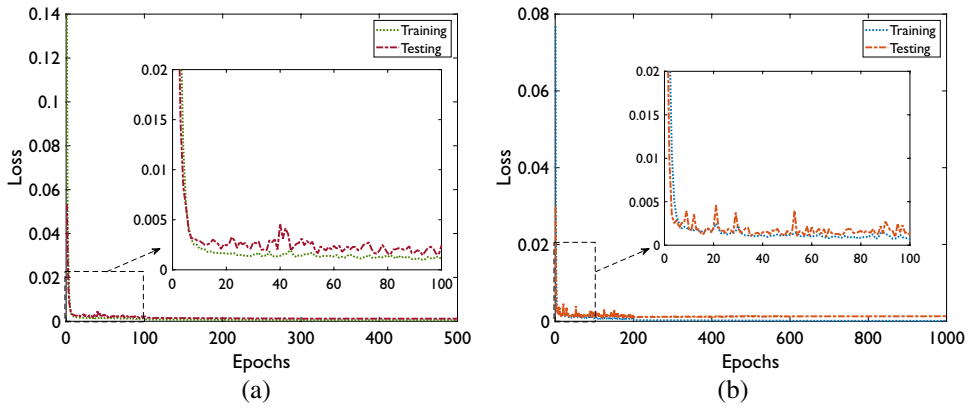

Fig. 4 Variation of the loss function during training and validation as a function of number of epochs, while predicting the (**a**) fracture strength and (**b**) power output of Silicon

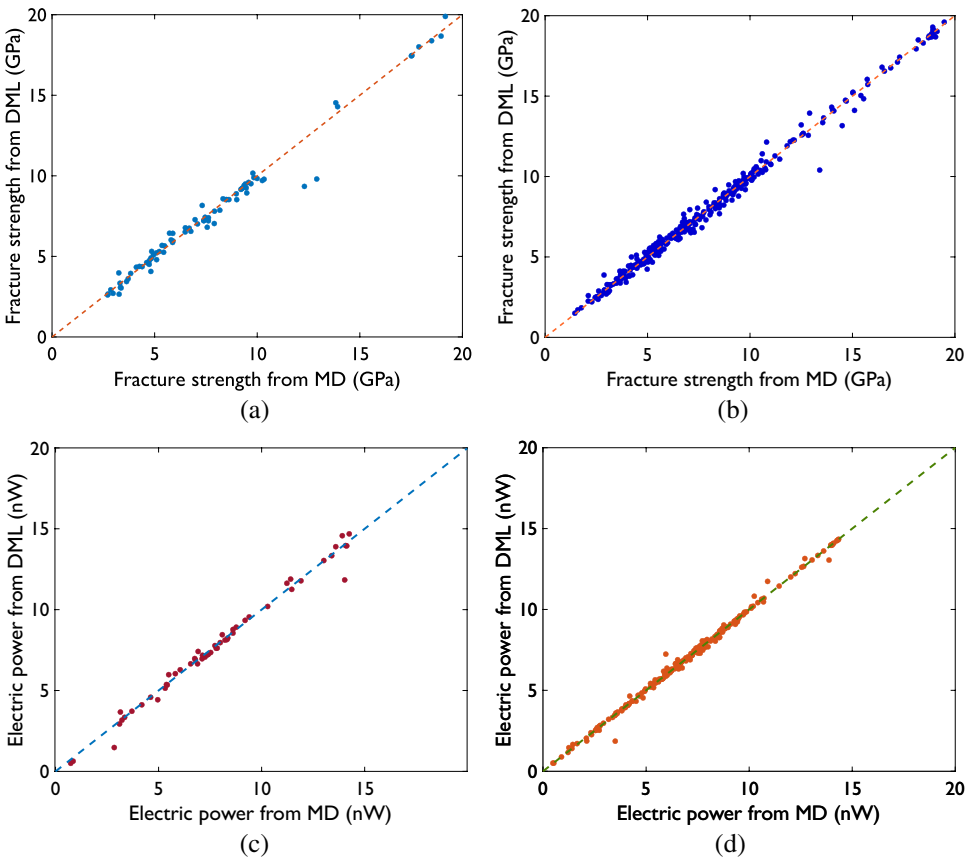

Fig. 5 Fracture strength of Silicon plotted as predicted from the proposed DML model vs. true values based on the MD simulations, for the (**a**) test and (**b**) train data sets. Similarly, the power output of Silicon plotted as predicted from the proposed DML model vs. true values based on the MD simulations, for the (**c**) test and (**d**) train data sets

plotted as expected vs. actual values, for sample sets used while training and testing, as illustrated in Fig. 5a, b, respectively, where the actual/true values are the outcomes of MD simulations. In the similar manner, the MD and predicted values during the testing and training of data sets for power output are plotted, as shown in Fig. 5c, d.

It is observed that the performance of the developed models for predicting the fracture strength and the electric power of Silicon domain are good. However, a few data points deviate from the reference values taken from MD simulations. According to Fig. 5a, b, a maximum deviation of 29.4% in the predicted fracture strength results when considering an edge crack size equal to $0.025w$ at 45° orientation is noticed during testing. Whereas, during training, it is found to be 17.81% with an initial edge crack size of $0.4w$ at 45° orientation. Similar maximum deviation of 18.53% in the predicted electric power is noticed during testing for a center crack of size $0.025w$ oriented at 45°, and 17.72% with an edge crack of length $0.1w$ oriented at 60° during training, see Fig. 5c, d. A trained DNN is referred to as a DML model from here onwards. The resulting DML model is verified

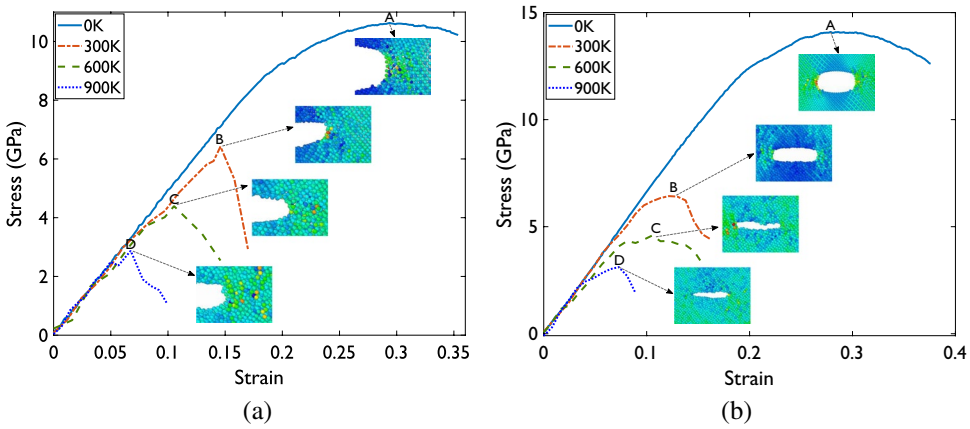

Fig. 6 Variation of the stress as a function of strain at temperatures equal to: 0 K, 300 K, 600 K and 900 K, considering an initial (**a**) edge crack of size $0.4w$ located at the mid-height and (**b**) a center crack of size $0.3w$, located in the middle of the domain; and oriented along the horizontal axis. A closeup of the atomic configuration around the crack tip at the stress peaks, i.e. at points A, B, C and D are also shown

using a 10-fold cross-validation to confirm its accuracy and robustness.

To summarize, the data for training and testing the developed DML model are generated with the help of MD simulations. In total 670 simulations, by varying the crack size, orientation, type and temperature are performed to generate the data for training and testing the developed ANN models. The fracture strength and electric power considering initial cracks are simulated using the `COMB` potential function, which accounts for multiple fields, such as: mechanical, thermal and electric fields. The considered multiple fields represents the actual physics of Silicon solar cells. Therefore, a lot of choice in the selection of potential functions for solar cells is not possible. Furthermore, the performed simulations are believed to be sufficient for estimating the fracture strength and electric power of Silicon-based solar cells in the presence of an arbitrary crack. Therefore, the developed DML model can predict the above parameters considering an initial crack. This will avoid executing MD codes every time when there is change in domain parameters, which saves a significant amount of computational time.

3 Results and discussion

In the present study, the stress at the initial bond break is chosen to determine the fracture strength of Silicon-based PV solar cells and total generated electric power at that instant, respectively. The above parameters are found to be significantly influenced by the crack size, position, and orientation, apart from the operating temperature of the solar cells.

3.1 Fracture strength

3.1.1 Deformed configurations

The variation of stress as function of strain at temperatures equal to 0 K, 300 K, 600 K and 900 K, considering an edge crack of length $0.4w$ located at the mid-height and a center crack of dimension $0.3w$; positioned at the centre of the domain and oriented along the horizontal axis are plotted in Fig. 6a, b, respectively. Furthermore, closeups of the deformed configuration around the crack tip at the stress peaks, i.e. at points A, B, C and D are also shown.

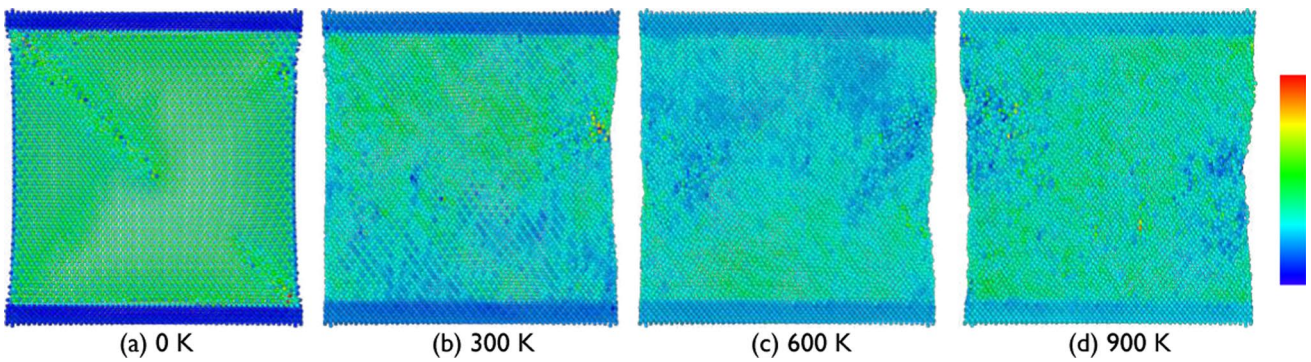

Fig. 7 Distribution of stress along the applied load direction at the instant of first bond break in the pristine Silicon domain at temperature equal to (**a**) 0 K, (**b**) 300 K, (**c**) 600 K and (**d**) 900 K

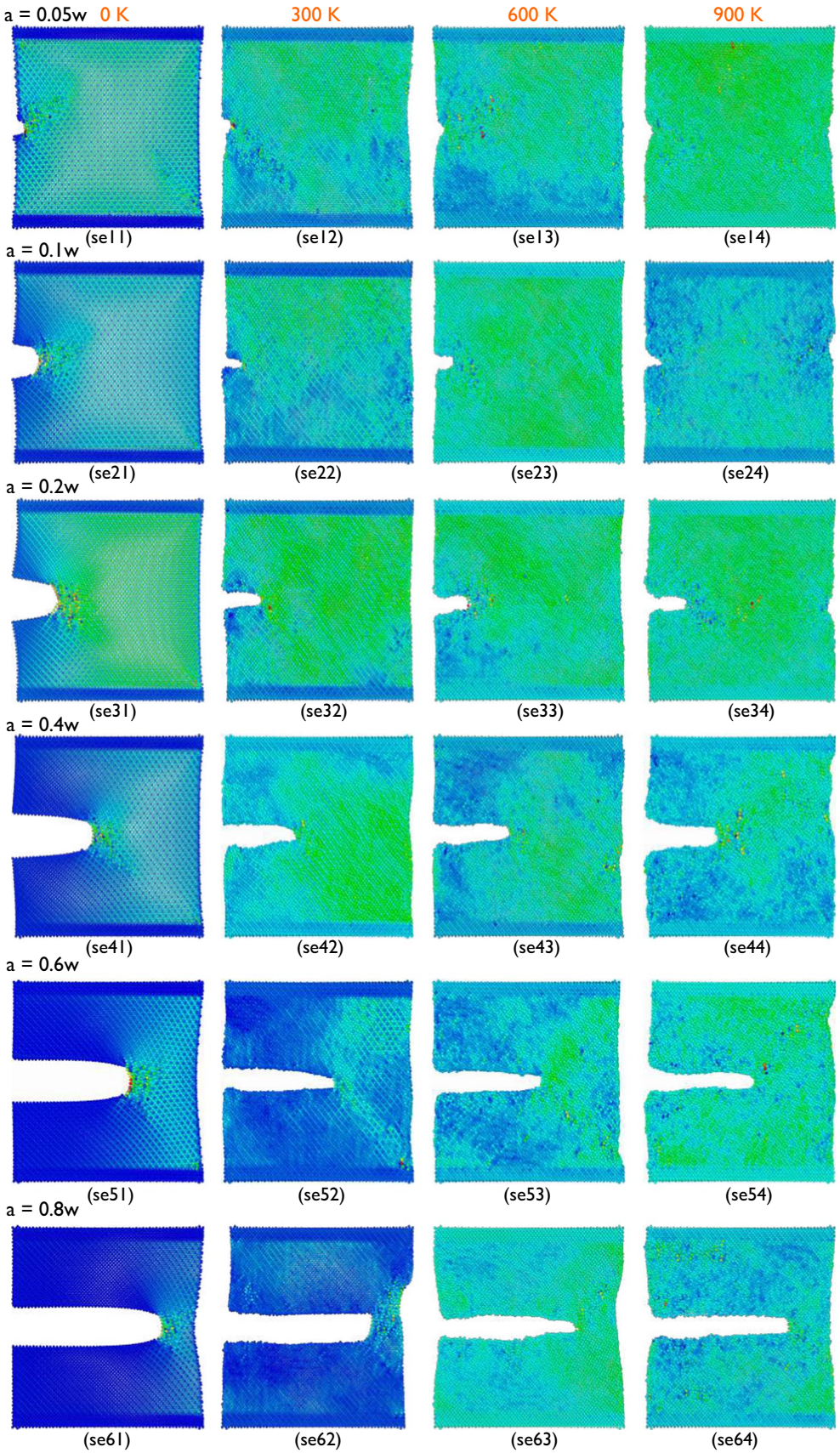
a = 0.05w
0 K
300 K
600 K
900 K
(se11)
(se12)
(se13)
(se14)
a = 0.1w
(se21)
(se22)
(se23)
(se24)
a = 0.2w
(se31)
(se32)
(se33)
(se34)
a = 0.4w
(se41)
(se42)
(se43)
(se44)
a = 0.6w
(se51)
(se52)
(se53)
(se54)
a = 0.8w
(se61)
(se62)
(se63)
(se64)

◂**Fig. 8** Distribution of stress along the applied load direction considering an initial edge crack in the Silicon domain. The distribution at temperatures equal to 0 K, 300 K, 600 K and 900 K are plotted in the first, second, third and fourth columns, respectively. Where as, distribution considering initial crack size equal to 0.05w, 0.1w, 0.2w, 0.4w, 0.6w and 0.8w are plotted in the first, second, third, fourth, fifth, and sixth rows, respectively

According to Fig. 6, all the curves are observed to follow a similar pattern, where the peak stresses indicating the fracture strength of Silicon are noticed to gradually decrease with raise in temperature. This is expected because the thermal mobility of atoms at high temperatures causes the fracture strength to drop as temperature rises. Furthermore, the elastic modulus of Silicon estimated from the MD simulations is found to be ≈90 GPa and the simulation setup is further extended to predict the fracture strength of Silicon considering various combinations of size and positioning of the crack along with the domain temperature.

The distribution of stress along the direction of applied load at the instant of first bond break in pristine Silicon domain at a temperature equal to 0 K, 300 K, 600 K and 900 K are shown in Fig. 7a–d. Increase in atomic vibrations due to the temperature increase is evident in Fig. 7. As a result, the deformed configurations are observed to deform in the lateral direction, inspite of the boundary conditions to suppress the lateral motion. This is mainly due to increase in thermal energy with increase in temperature, leading to accelerated random atomic vibrations, see Fig. 7c, d. Hence, the maximum stress is observed to be a decreasing function of temperature.

The distribution of stress along the direction of applied load considering an edge crack in the Silicon domain, at temperatures ranging from 0 K to 900 K in steps of 300 K are, respectively, plotted in the columns: one, two, three, and four of Fig. 8. The same distribution considering crack length equal to 5%, 10%, 20%, 40%, 60%, and 80% of width of the domain are plotted in the first, second, third, fourth, fifth, and sixth rows, respectively. Increase in atomic motion with temperature is noticed. It is observed that with an increase in the crack size as well as domain temperature, the fracture strength is decreased. The internal resistance of Silicon reduces when the initial crack size is increased, which further reduces at higher temperatures.

Similarly, the distribution of stress along the direction of applied load considering an initial center crack in the Silicon domain, at temperatures ranging from 0 K to 900 K, in steps of 300 K are, respectively, plotted in the columns: one, two, three, and four of Fig. 9. The same distribution with an initial crack orientation equal to zero degree, thirty degrees, forty five degrees, and sixty degrees are plotted in the first, second, third, and fourth rows, respectively. When the initial crack size and domain temperature are increased, the fracture strength is found to be decreased.

3.1.2 Comparison of MD and DML studies

With respect to the crack size factor, the fracture strength from MD and DML investigations is compared at temperatures of 0 K, 300 K, 353 K, 600 K, and 900 K., considering an edge crack positioned along 0° and 30° directions, is shown in Fig. 10. An observation of Fig. 10a, b indicates that the DML model findings and the MD simulation results match well. Furthermore, a maximum average error of 6.83% is observed at 900 K. The distribution of fracture strength with respect to the temperature at different crack sizes, considering the initial edge crack oriented along 0° and 30° is plotted in Fig. 11. According to Fig. 11a, b, the fracture strength is observed to be a decreasing function of temperature and crack size. Furthermore, it approaches the endurance limit at higher temperatures, particularly at 900 K, irrespective of the crack size considered at the beginning, see Fig. 11b.

The fracture strength is found to decrease by increasing the initial crack size. A smooth and almost linear reduction is noticed when temperature is equal to zero Kelvin for all crack orientations, see Fig. 10. However, a sudden drop from no crack to small initial crack of size 0.05w is noticed at higher temperatures. The trend is observed to be almost similar for all crack orientations. However, the drop is seen to be increasing with raise in crack orientation, see Fig. 11.

A comparison of fracture strength from MD and DML investigations, at temperatures equal to 0 K, 300 K, 353 K, 600 K and 900 K, considering an initial center crack oriented along 0°, 30°, 45° and 60° directions is shown in Fig. 12. For the given crack size, the fluctuation of fracture strength is seen to decrease with raise in temperatures up to 600 K. This indicates that the fracture strength is significantly effected by the crack size and temperature up to 600 K at a given constant mechanical strain externally applied. Whereas, beyond 600 K, and up to 900 K, it is observed that this range remained almost constant, indicating that there is no proportionate change then after, irrespective of crack size. The fracture strength drops at higher temperatures as a result of significant thermal fluctuations. The kinetic energy and thus the total energy of atoms increases with temperature, leading to unstable conditions, resulting in the bonds breaking at relatively lower external loads. Thus, a rapid decay in the fracture strength of Silicon is observed.

Similar to the edge crack model, the fracture strength of center crack model is found to drop with increase in crack length, with a smooth and almost linear reduction when temperature is equal to zero kelvin for all initial crack orientations. However, at 0 K, the fracture strength of Silicon domain with center crack is found to be higher than the domain with an edge crack. On the other hand, a sudden drop from no crack to initial crack of size 0.05w is noticed at higher temperatures for all orientations, see Fig. 12.

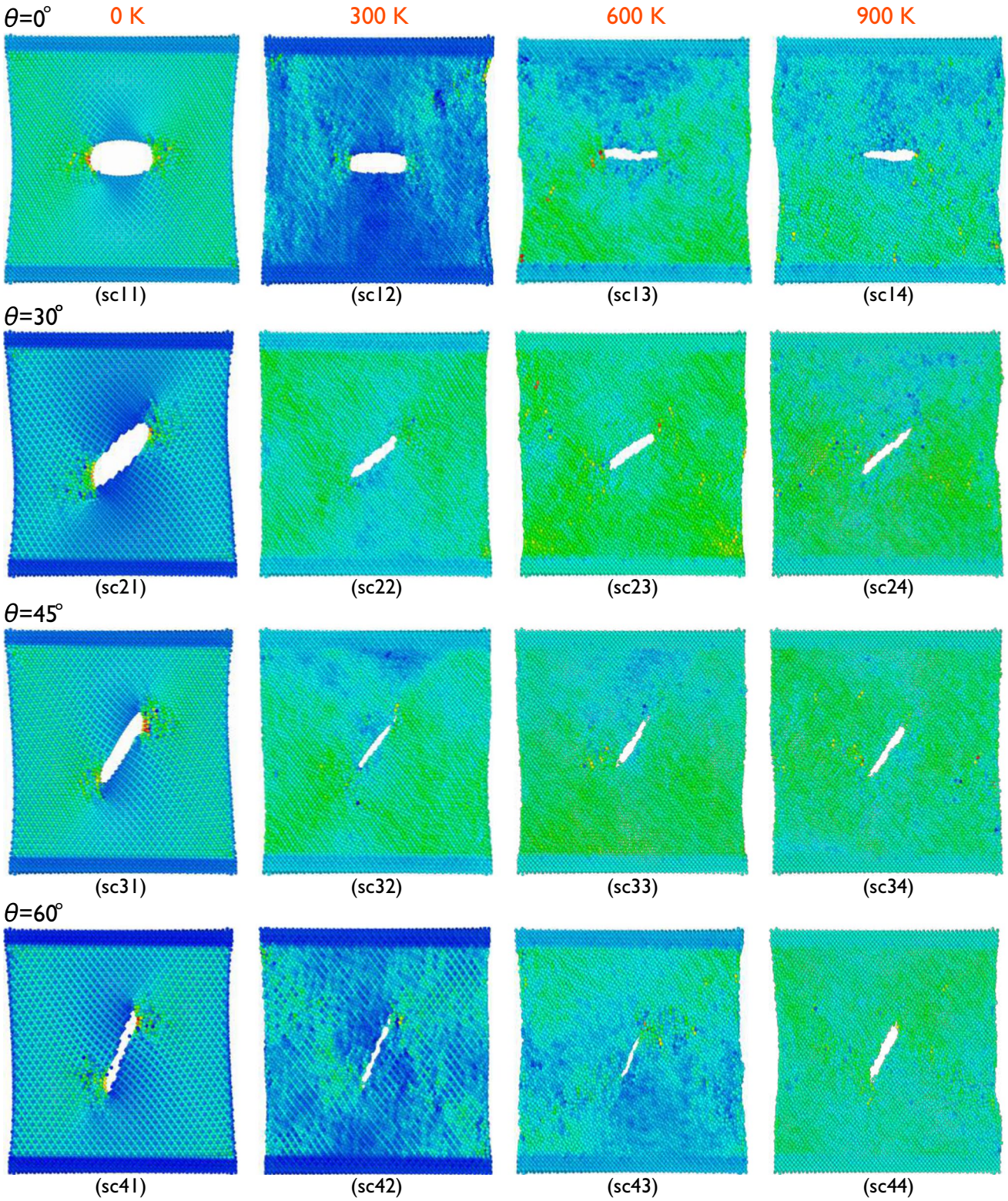

Fig. 9 Distribution of stress along the applied load direction considering an initial center crack in the Silicon domain. The distribution at temperatures equal to 0 K, 300 K, 600 K and 900 K are plotted in the first, second, third and fourth columns, respectively. Where as, distribution considering initial crack orientation equal to 0°, 30°, 45°, and 60° are plotted in the first, second, third, and fourth rows, respectively

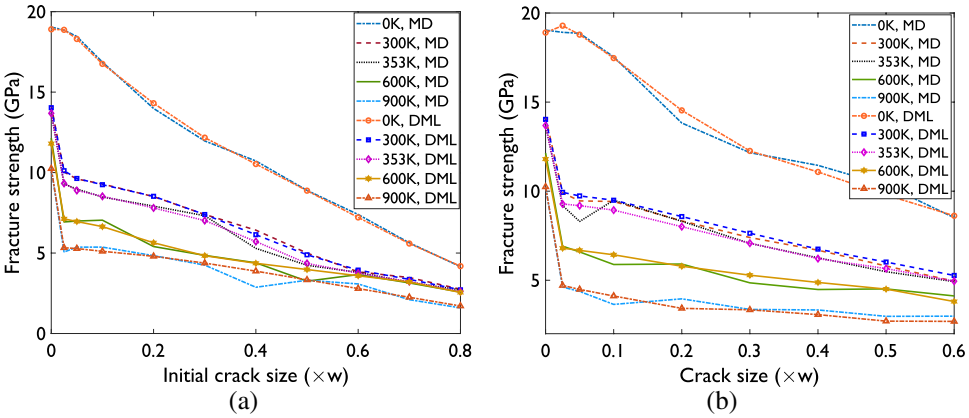

Fig. 10 Comparison of fracture strength results from MD and DML studies as a function of crack size, at temperatures 0 K, 300 K, 353 K, 600 K and 900 K, considering the initial edge crack oriented along (**a**) 0° and (**b**) 30° directions

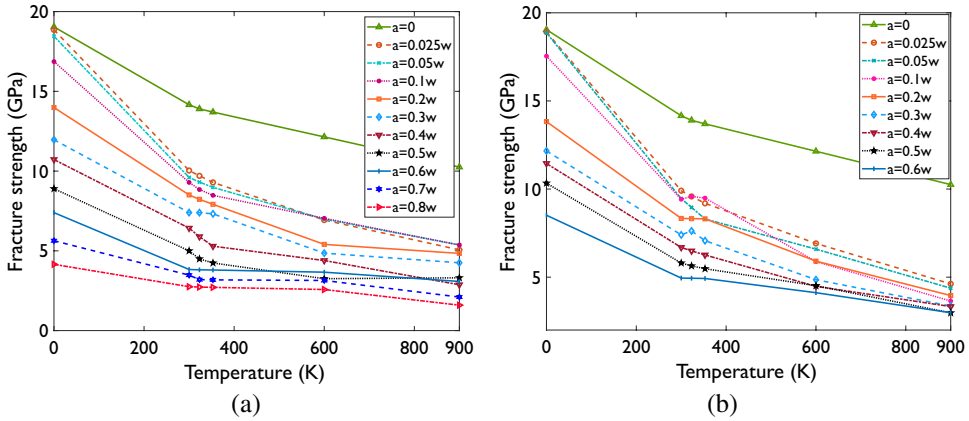

Fig. 11 Distribution of fracture strength results from MD simulations as a function of temperature at different crack sizes, considering the initial edge crack oriented along (**a**) 0° and (**b**) 30° directions

Whereas, the drop is found to be reducing as the initial crack orientation increases.

In addition, distribution of fracture strength calculated using MD simulations as a function of domain temperature at various initial crack sizes is given in Fig. 13, taking into account the central crack oriented along 0°, 30°, 45°, and 60° directions. According to Fig. 13, an exponential decrease in fracture strength is seen as the domain temperature and crack size increases, approaching an endurance limit around 4.5 GPa, at higher temperatures, particularly at 900 K, irrespective of the initial crack crack size and orientation, see Fig. 13. However, the fracture strength of pristine Silicon is observed to be much higher than the above endurance limit with initial crack. As a result, it is clear that the presence of initial crack influences the fracture strength of Silicon.

3.1.3 Influence of crack location and orientation

To predict the influence of position of crack on the fracture strength of Silicon, a comparison of the fracture strength variation in relation to the crack orientation, considering an edge and center cracks of size $0.3w$ at 0 K, 300 K, 353 K and 600 K, is shown in Fig. 14. According to Fig. 14a, Silicon fracture strength in the presence of center crack is more than ≈15% as compared to the same domain with an edge crack. The trend is continued even at higher temperatures, see Fig. 14b, although the difference is small as compared to 0 K. Based on Fig. 14, it is found that with increase in crack orientation, the fracture strength increases. Additionally, as the orientation increases, the time elapsed for the first bond to collapse also increases. This reveals that Silicon absorbs more stresses as crack orientation increases, which accounts for the rise in fracture strength with orientation angle. Furthermore, the crack will experience mixed mode loading (mode I and mode II) when it's orientation angles are other than 0°, leading to anisotropy in elasticity. The crack growth is driven by the effective stress intensity factor, calculated as $K_{\text{eff}} = \sqrt{K_{\text{I}}^2 + K_{\text{II}}^2}$. Higher fracture strength of the Silicon results from K_{eff}, which is greater than K_I. Regardless of the orientation angle, the fracture strength is noticed to decrease with the increase in temperature.

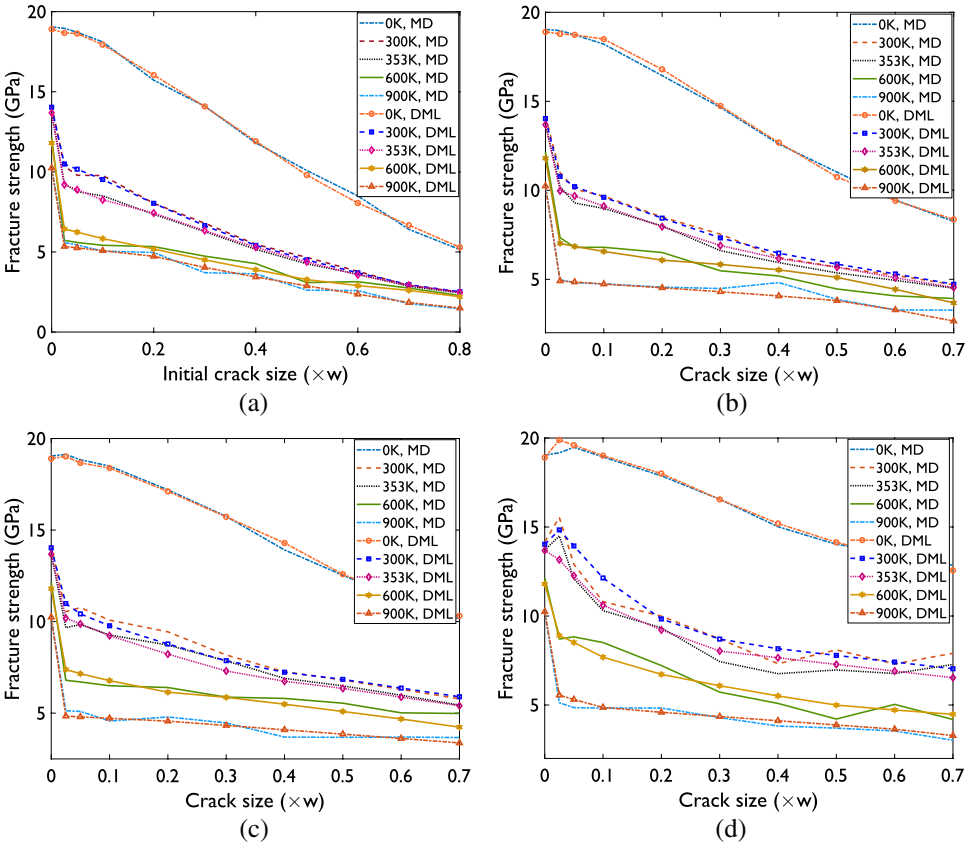

Fig. 12 Comparison of fracture strength results from MD and DML studies as a function of crack size, at temperatures 0 K, 300 K, 353 K, 600 K and 900 K, considering the initial center crack oriented along (**a**) 0° (**b**) 30° (**c**) 45° and (**d**) 60° directions

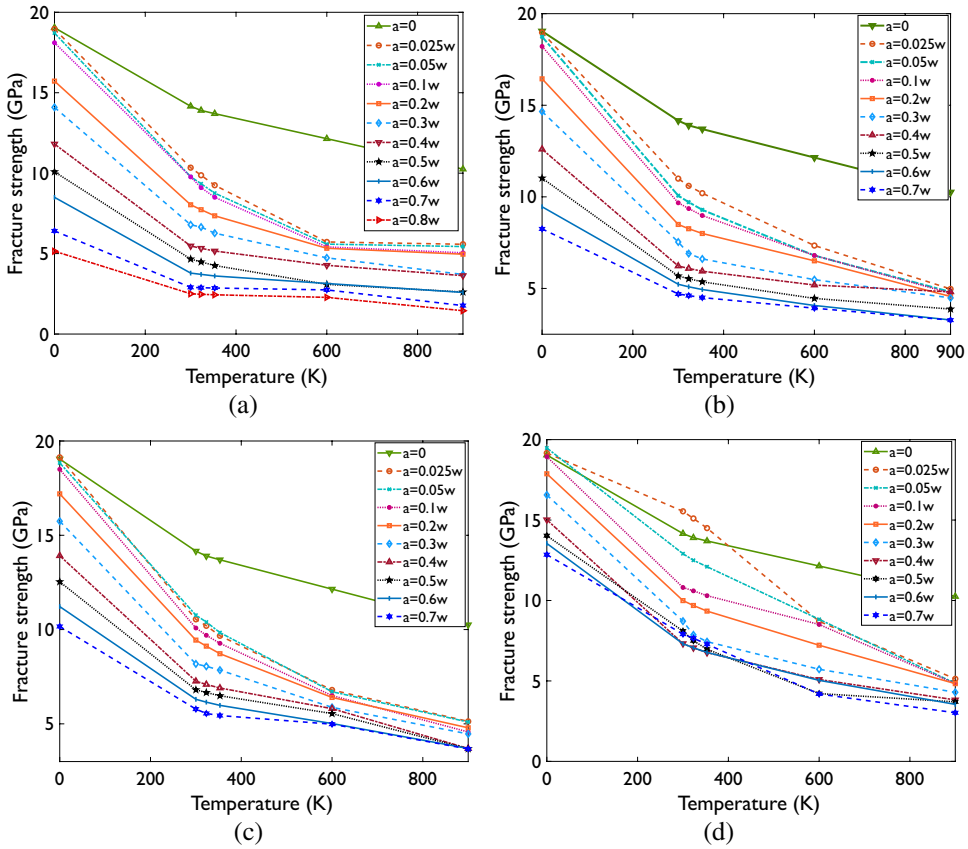

Fig. 13 Distribution of fracture strength results estimated from MD simulations as a function of temperature at different crack sizes, considering the initial center crack oriented along (**a**) 0°, (**b**) 30°, (**c**) 45° and (**d**) 60° directions

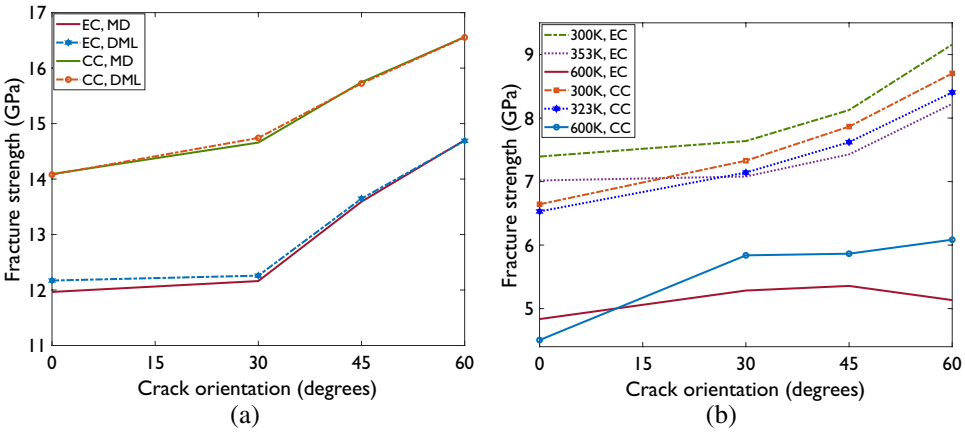

Fig. 14 Influence of crack orientation on the fracture strength. **a** Comparison of the variation of fracture strength results from MD and DML studies with respect to the crack orientation, considering an initial edge and center cracks of size $0.3w$ at 0 K. **b** Similar comparison without DML results at higher temperatures: 300 K, 353 K and 600 K

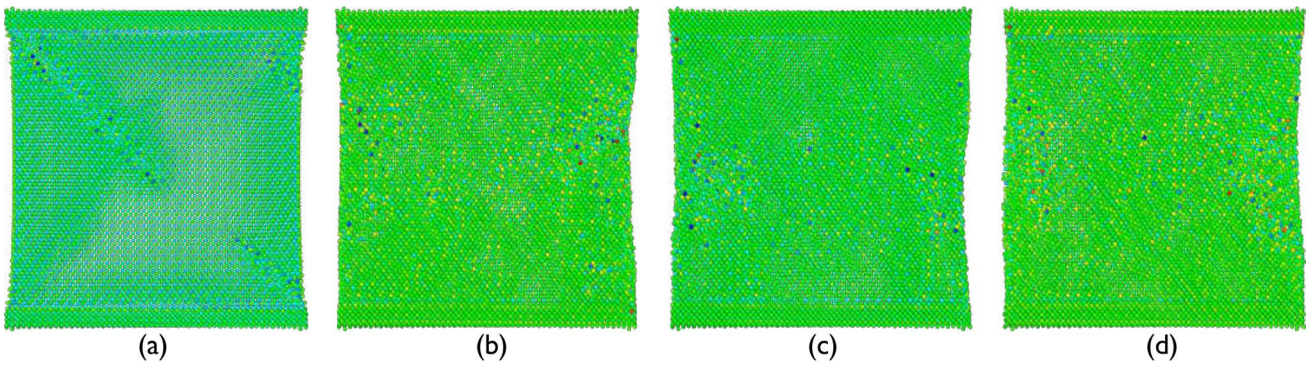

Fig. 15 Distribution of electric charge in pristine Silicon domain at temperatures equal to (**a**) 0 K, (**b**) 300 K, (**c**) 323 K and (**d**) 353 K

3.2 Power output

Considering the operating temperatures of Silicon PV cells, the influence of initial cracks on the power output characteristics are investigated under operating temperatures up to 353 K. Distribution of electric charge at the instant of first bond break in pristine Silicon domain at temperatures equal to 0 K, 300 K, 323 K and 353 K is shown in Fig. 15. In the region of damaged areas, including the boundaries, it has been found that the charge distribution fluctuates significantly with temperature. Additionally, it is seen that the specimen fails through brittle fracture along the borders towards the end of the simulation. This is due to the fact that damage will start in the over stressed regions, which in this instance are near to the boundaries, in the absence of initial flaws or imperfections like cracks.

The distribution of electric charge considering initial edge crack in the Silicon domain, at temperatures equal to 0 K, 300 K, 323 K and 353 K, are, respectively, plotted in the columns: one, two, three, and four of Fig. 16. The same distribution considering crack sizes equal to 5%, 10%, 20%, 40%, 60%, and 80% of width of the domain are plotted in the first, second, third, fourth, fifth, and sixth rows, respectively. The atoms near the crack tip are subjected to high stresses, see Fig. 8, and had increased random motions with temperature leading to the increase in the charge accumulation near the crack tip. The randomness further increased with increase in crack size, resulting in further charge accumulation, see Fig. 16.

The distribution of electric charge considering an initial center crack in the Silicon domain, at temperatures equal to 0 K, 300 K, 323 K and 353 K, are, respectively, plotted in the first, second, third and fourth columns of Fig. 17. The same distribution with various aforementioned crack orientations is plotted in the rows: one, two, three and four, respectively. Similar to the edge crack case, the stresses near the crack tip are relatively higher leading to random movement of atoms and thus the charge accumulation. Whereas, with crack orientation, this randomness is reduced leading to the decrease in charge accumulation and thus improving the performance of solar cell, the details of which are discussed in the upcoming sections.

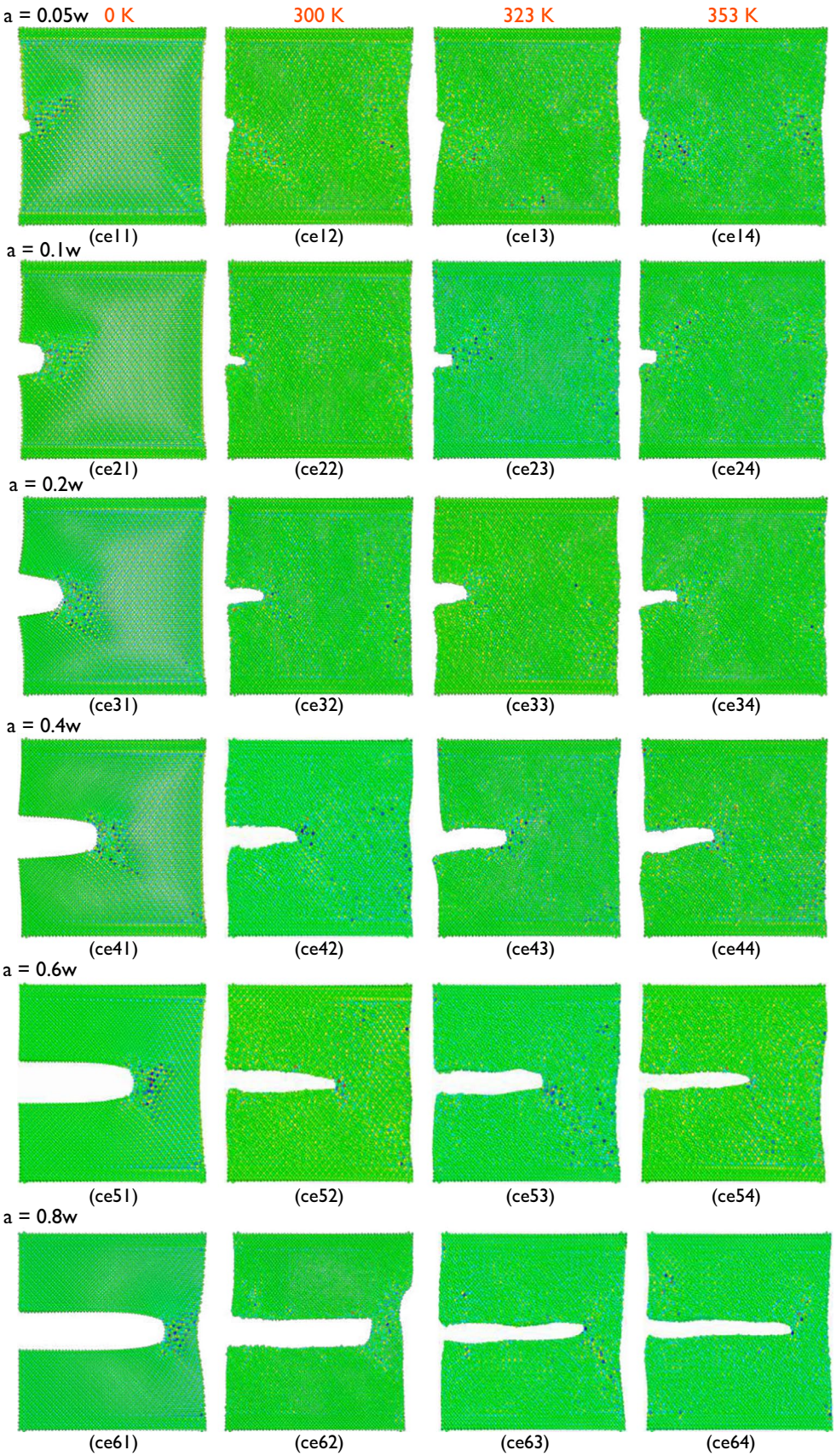

Fig. 16 Variation of electric charge in the solar cell considering an initial edge crack in the Silicon domain. The distribution at temperatures equal to 0 K, 300 K, 323 K and 353 K are plotted in the first, second, third and fourth columns, respectively. Where as, distribution considering initial crack size equal to $0.05w$, $0.1w$, $0.2w$, $0.4w$, $0.6w$ and $0.8w$ are plotted in the first, second, third, fourth, fifth, and sixth rows, respectively

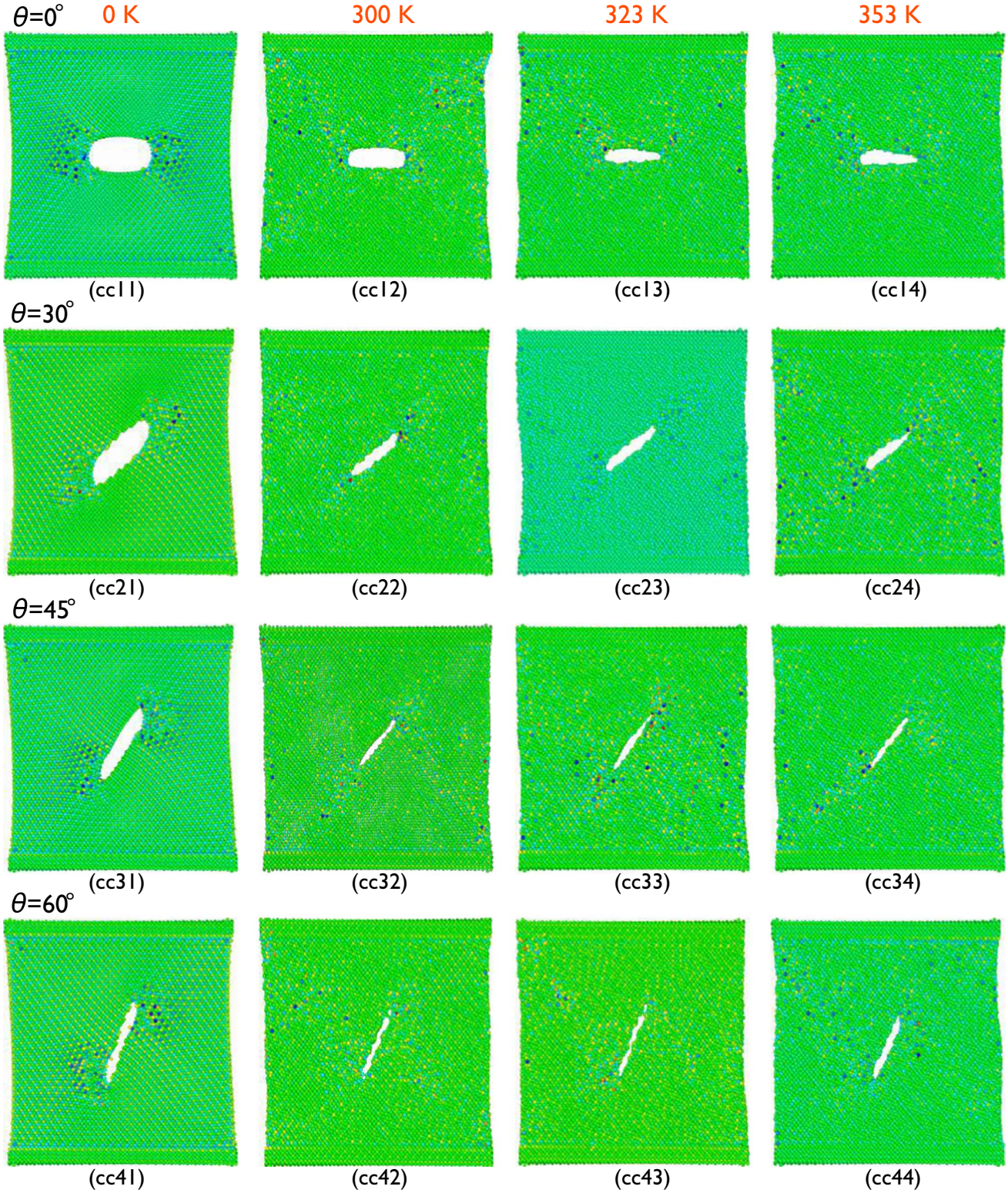

Fig. 17 Variation of electric charge in the solar cell considering an initial center crack in the Silicon domain. The distribution at temperatures equal to 0 K, 300 K, 323 K and 353 K are plotted in the first, second, third and fourth columns, respectively. Where as, distribution considering initial crack orientation equal to 0°, 30°, 45°, and 60° are plotted in the first, second, third, and fourth rows, respectively

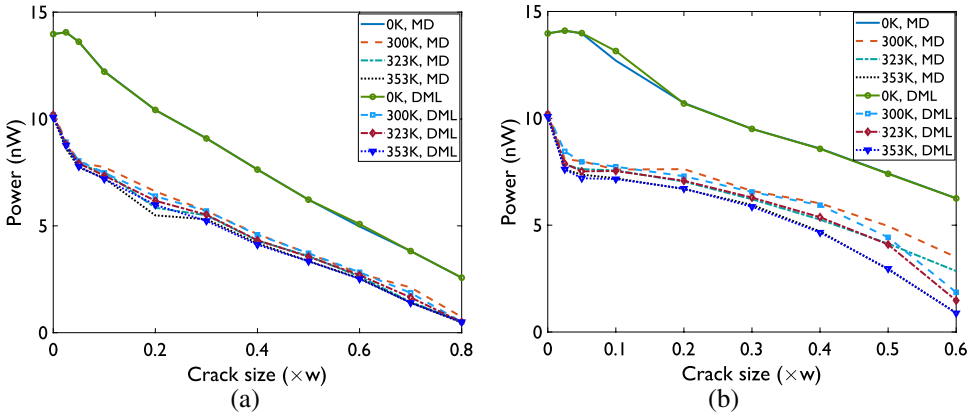

Fig. 18 Comparison of electric power results from MD and DML studies as a function of crack size, at temperatures 0 K, 300 K, 323 K, and 353 K, considering the initial edge crack oriented along (**a**) 0° and (**b**) 30° directions

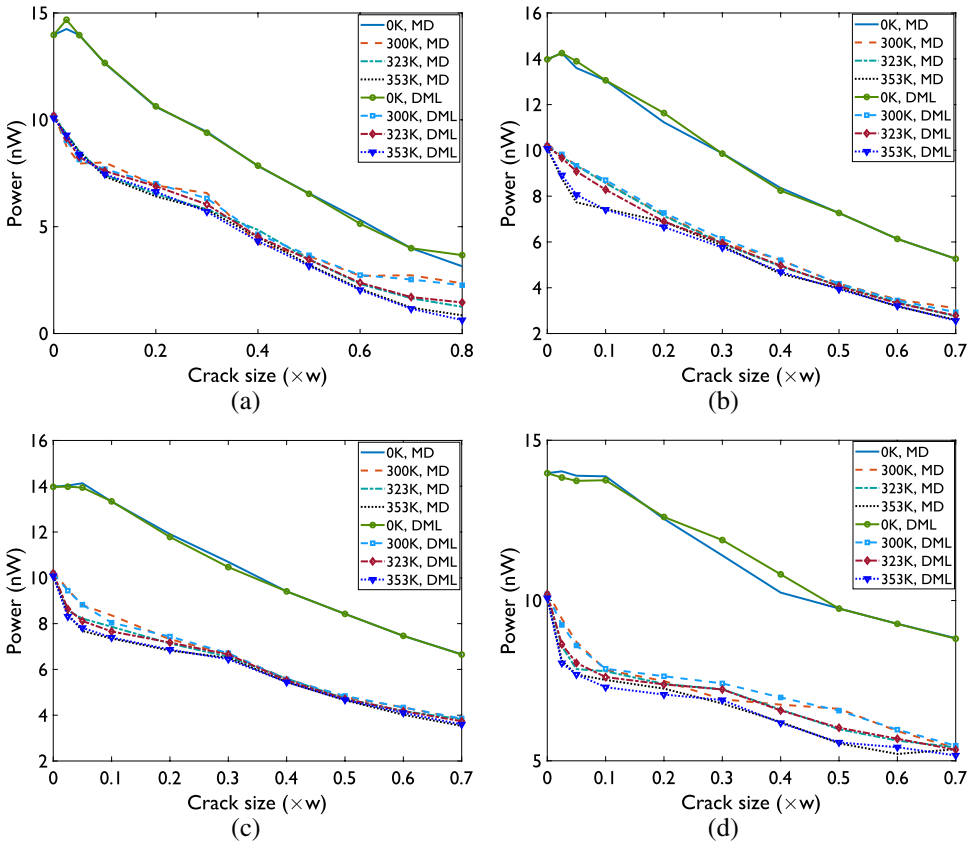

Fig. 19 Comparison of electric power results from MD and DML studies as a function of crack size, at temperatures 0 K, 300 K, 323 K, and 353 K, considering the initial center crack oriented along (**a**) 0°, (**b**) 30°, (**c**) 45°, and (**d**) 60° directions

3.2.1 Comparison of MD and DML results

A comparison of electric power results from MD and DML studies as a function of crack size, at temperatures equal to 0 K, 300 K, 323 K, and 353 K, considering the initial edge crack oriented along 0° and 30° directions, is shown in Fig. 18. An observation of Fig. 18a, b shows that the DML model results and the outcomes of the MD simulations are closely aligned, where a maximum error of 18.53% is noticed with only 2.6% of total cases having error percent greater than ten. As the crack length increases, the power output is seen to decrease. A smooth and almost linear reduction is noticed when temperature is equal to zero kelvin for all types of crack orientations. However, a sudden drop from no crack to small initial crack of size $0.05w$ is noticed at higher temperatures. The trend is noticed to be almost similar for all crack orientations. However, the drop is noticed to be increasing with increase in orientation angles. Furthermore, it is observed that the electric power decreased with increase in temperature.

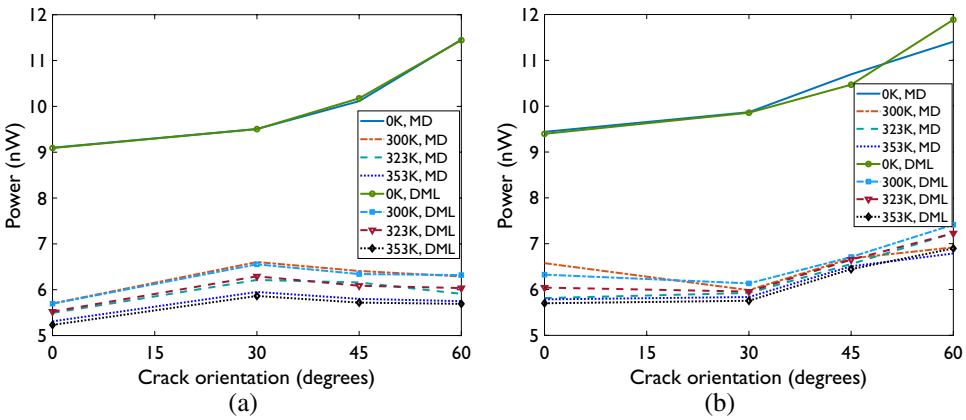

Fig. 20 Influence of crack orientation on the electric power. Comparison of the variation of electric power results from MD and DML studies with respect to the crack orientation, considering an initial crack size of 0.3w and 0 K, 300 K, 323 K, 353 K temperatures: (**a**) edge crack (**b**) center crack

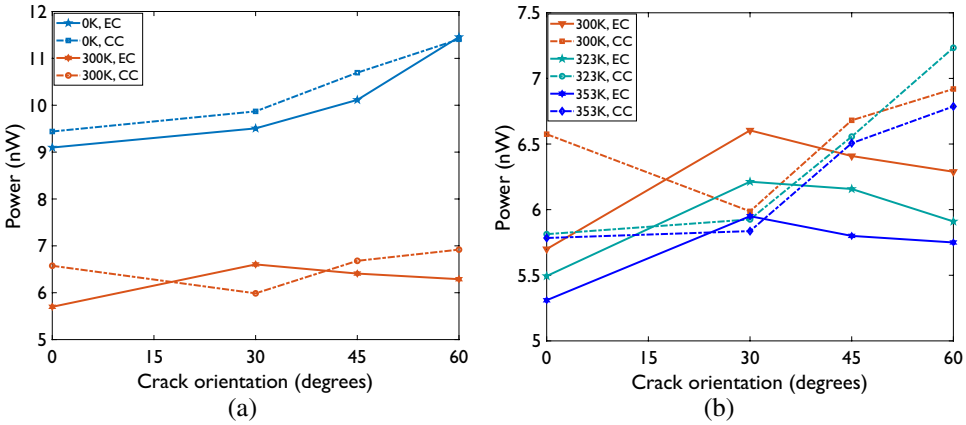

Fig. 21 Influence of crack orientation on the electric power. Comparison of the variation of power output results from edge and center crack studies with respect to the crack orientation, considering an initial crack size of 0.3w: (**a**) 0 and 300 K (**b**) 300, 323, 353 K

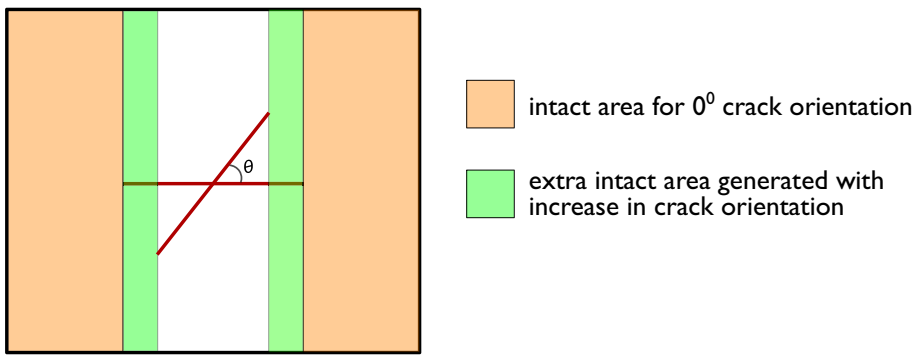

Fig. 22 Schematic showing the increase in intact area with increased crack orientation, for a given crack size

The above procedure is extended to investigate the influence considering a center crack. A comparison of electric power results from MD and DML studies as a function of crack size, at temperatures equal to 0 K, 300 K, 323 K, and 353 K considering the initial center crack oriented along 0°, 30°, 45° and 60° directions is shown in Fig. 19. Similar to the edge crack model, the power output witnessed a decrease by increasing crack size. A smooth and almost linear reduction is observed when the temperature is equal to zero kelvin for all the above orientation angles. However, at zero kelvin, the power output of Silicon domain with center crack is found to be higher than the domain with an edge crack. On the other hand, a sudden drop from no crack to small initial crack of size 0.05w is noticed at higher temperatures for all orientations, see Fig. 19. Whereas, this drop is found to reduce with increase in initial crack orientation.

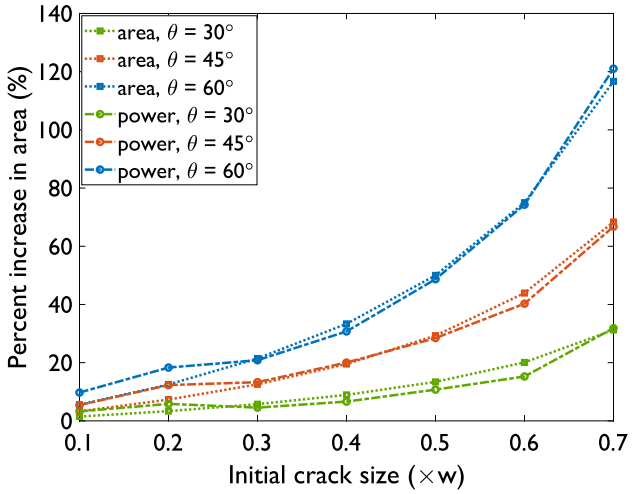

Fig. 23 Comparison of percentage increase in the intact area and hence the corresponding increase in electric power with increased crack orientation and crack size at 0 K

In order to predict the influence of initial edge and center cracks on the electric power of Silicon solar cell, a comparison of the variation of electric power with respect to the crack orientation, considering an initial edge and center cracks of size 0.3w at 0 K, 300 K, 323 K and 353 K, is shown in Fig. 20. The electric power is observed to be decreasing with increase in temperature. As the temperature increases, the random movement of atoms near the crack tip increases leading to increase in charge accumulation, see Fig. 16. As a result, the large concentrations of electric potential energies around the tip are wasted, which lowers the output of useful electric power. Furthermore, it is also observed that the electric power increased with crack orientation in both edge and center cracks. This is due to the reason that as the crack is oriented, it is observed that the charge accumulation reduced as compared to 0° crack case, see Fig. 17. As a result the net electric potential energy available for electric power increases leading to enhanced performance of the solar cell.

3.2.2 Impact of crack location and orientation

The impact of location and orientation of crack on power output is observed by plotting electric power with crack orientation as shown in Fig. 21a, b. It is observed that at 0 K, the electric power of Silicon domain with a center crack is ≈ 3.8% higher as compared to the same domain with an initial edge crack. In most of the cases, center crack case experienced higher electric power than edge crack case. At higher temperatures, due to the random fluctuations of electric charge and thus the electric potential energies, the associated electric power had proportionate fluctuation which can be evidenced through Fig. 21b. Furthermore, as the orientation angle of these cracks increases, its effect on the power output decreases [7], as shown in Fig. 21. This is due to the reason that, as we increase the through crack orientation for the given crack size, availability of continuous material volume without any defect increases, see Fig. 22, leading to decrease in obstruction to the free flow of charge within the material. It can be observed that, as the crack orientation increases, the area/volume available for free flow of charges increases by an amount equal to that of the region highlighted in blue color, see Fig. 22. As a result, the chances of charge accumulation decreases and the performance enhances. At lower temperatures, it is observed that this percent increase in area available for free movement of charges is in line with the percent increase in electric power as shown in Fig. 23. The percentage increase in the power of Silicon domain with center crack is increasing with crack size and orientation and is in line with the corresponding percentage increase in the available area.

4 Conclusions

A framework has been proposed to estimate the electric power and fracture strength of a Silicon solar cell at the point of first bond break in the presence of an initial edge and center cracks considering their size, orientation, and the temperature of the cell. Fracture strength and the electric power are estimated through a combined molecular dynamic simulations and deep machine learning-based approach and the corresponding models have been developed. Four alternative crack orientation angles: 0°, 30°, 45°, and 60° and various initial crack sizes, ranging from 2.5 to 80% of the domain size are adopted in the simulations. The cell temperature has also been varied between 0 K and 900 K in steps of 300 K along with two other operating temperatures, namely: 323 K and 353 K while dealing with the electric power study. Thus, a total of 268 and 402 samples have been generated through the MD simulations to estimate the electric power and fracture strength of Silicon solar cell.

The outcomes of the MD simulations are used to train the DML model. When results from DML and MD are compared, it is found that the DML outputs closely match the outcomes of the MD simulations. In comparison to the outcomes of MD simulations, the maximum deviation in the DML model predictions is found to be 18.53% for electric power and 29.4% for fracture strength, respectively.

Based on the findings, the impact of different crack parameters on fracture strength and electric power is examined. It has been established that when the crack size increases, both electric power and fracture strength decreases. The decrease is particularly noticeable for tiny crack sizes when compared to the pristine Silicon. Furthermore, the drop increases with increase in temperature.

On the other hand, with increase in crack orientation, the fracture strength and electric power are also found to be increasing.

A drop of ≈ 40-50% in electric power has been reported with increase in temperature, irrespective of crack size and crack orientation. Whereas, at a given temperature and crack orientation between 0° and 60° and initial crack sizes varying between $0.1w$ and $0.5w$, a linear increase in electric power has been reported. For instance, for an initial crack size equal to $0.2w$ and a crack orientation angle varying between 0° and 60°, the electric power is increased by 20% at a given temperature. For crack sizes greater than $0.5w$, the electric power improved exponentially.

The methods proposed in this work can be used to estimate the fracture strength and electric power of the Silicon solar cells. Significant computational times can be saved by using the developed DML model for estimating the fracture strength as well as electric power output of Silicon solar cell considering arbitrary size and orientation of initial cracks, as compared to MD simulations.

Acknowledgements Budarapu is grateful to Indian Institute of Technology Bhubaneswar for sponsoring this research through grant number SP-097.

Data availibility Since the raw/processed data are also used in an ongoing study, it is not currently possible to share them in order to replicate these results.

Declarations

Conflicts of interest The authors declare no conflicts of interest.

References

1. B. Javvaji, P.R. Budarapu, M. Paggi, X. Zhuang, T. Rabczuk, Fracture properties of graphene-coated silicon for photovoltaics. Adv. Theory Simul. **1**(12), 1800097 (2018)
2. S. Pingel, Y. Zemen, O. Frank, T. Geipel, J. Berghold, Mechanical stability of solar cells within solar panels. Proc. of 24th EUPVSEC, 3459–3464 (2009)
3. A. M. Gabor, M. Ralli, S. Montminy, L. Alegria, C. Bordonaro, J. Woods, L. Felton, M. Davis, B. Atchley, T. Williams, Soldering induced damage to thin si solar cells and detection of cracked cells in modules. In 21st European Photovoltaic Solar Energy Conference, 4–8 (2006)
4. C.P. Chen, *Fracture strength of silicon solar cells* (Jet Propulsion Laboratory, California Institute of Technology, 1979)
5. Mahmoud Dhimish, Violeta Holmes, Mark Dales, Bruce Mehrdadi, Effect of micro cracks on photovoltaic output power: case study based on real time long term data measurements. Micro Nano Lett. **12**(10), 803–807 (2017)
6. D. C. Nguyen, Y. Ishikawa, Y. Uraoka, Recover possibilities of potential induced degradation caused by the micro-cracked locations in p-type crystalline silicon solar cells. Progress in Photovoltaics: Res. Appl. **29**(4), 423–432 (2021)
7. Sarah Kajari-Schröder, Iris Kunze, Ulrich Eitner, Marc Köntges, Spatial and orientational distribution of cracks in crystalline photovoltaic modules generated by mechanical load tests. Solar Energy Mater. Solar Cells **95**(11), 3054–3059 (2011)
8. C. Buerhop-Lutz, T. Winkler, F. W. Fecher, A. Bemm, J. Hauch, C. Camus, C.J. Brabec (2017) Performance analysis of precracked pv-modules at realistic loading conditions. Proc. 33rd Euro. PV-SEC, 5CO, **8**, 1451–1456
9. M. Paggi, M. Corrado, M.A. Rodriguez, A multi-physics and multi-scale numerical approach to microcracking and power-loss in photovoltaic modules. Composite Struct. **95**, 630–638 (2013)
10. S.D.V.S.S. Varma Siruvuri, P.R. Budarapu, M. Paggi, Current-voltage characteristics of silicon based solar cells in the presence of cracks: Md simulations. Semiconductor Sci. Technol. **37**(2), 025011 (2021)
11. Przemyslaw Rupnowski, Bhushan Sopori, Strength of silicon wafers: fracture mechanics approach. Int. J. Fracture **155**(1), 67–74 (2009)
12. C. Funke, E. Kullig, M. Kuna, H. Joachim Möller, Biaxial fracture test of silicon wafers. Adv. Eng. Materials **6**(7), 594–598 (2004)
13. F. Kaule, W. Wang, S. Schoenfelder, Modeling and testing the mechanical strength of solar cells. Solar Energy Mater. Solar Cells **120**, 441–447 (2014)
14. Lv. Zhao, Anne Maynadier, Daniel Nelias, Stiffness and fracture analysis of photovoltaic grade silicon plates. Int. J. Solids Struct. **97**, 355–369 (2016)
15. M. Sander, S. Dietrich, et al, Influence of manufacturing processes and subsequent weathering on cell cracks in pv modules. 28th EU PVSEC, (2013)
16. G. Li, M.W. Akram, Y.i. Jin, X. Chen, C. Zhu, A. Ahmad, R.H. Arshad, X. Zhao, Thermo-mechanical behavior assessment of smart wire connected and busbarpv modules during production, transportation, and subsequent field loading stages. Energy **168**, 931–945 (2019)
17. F. Reil, J. Althaus, W. Vaaßen, W. Herrmann, K. Strohkendl (2010) The effect of transportation impacts and dynamic load tests on the mechanical and electrical behaviour of crystalline pv modules. In: Proc. 25h European PV Solar Energy Conference, 3989–3992
18. K. Yasutake, M. Iwata, K. Yoshii, M. Umeno, H. Kawabe, Crack healing and fracture strength of silicon crystals. J. Mater. Sci. **21**(6), 2185–2192 (1986)
19. S.E. Nikitin, V.V. Shpeizman, A.O. Pozdnyakov, S.I. Stepanov, R.B. Timashov, V.I. Nikolaev, E.I. Terukov, A.V. Bobyl, Fracture strength of silicon solar wafers with different surface textures. Materials Sci. Semiconductor Process. **140**, 106386 (2022)
20. V.A. Popovich, W. Geerstma, M. Janssen, I.J. Bennett, I.M. Richardson, Mechanical strength of silicon solar wafers characterized by ring-on-ring test in combination with digital image correlation. In: EPD Congress 2015, pages 241–248. Springer, (2015)
21. H. Seigneur, E. Schneller, J. Lincoln, H. Ebrahimi, R. Ghosh, A. M. Gabor, M. Rowell, V. Victor Huayamave, Microcrack formation in silicon solar cells during cold temperatures. In: 2019 IEEE 46th Photovoltaic Specialists Conference (PVSC), volume 2, pages 1–6. IEEE, (2019)
22. M. Wang (2019) Dynamic fracture of solar grade single crystalline silicon wafers. PhD thesis, Université de Lyon
23. Wei Wan, Changxin Tang, Jianjie Zhang, Lang Zhou, General molecular dynamics approach to understand the mechanical anisotropy of monocrystalline silicon under the nanoscale effects of point defect. Nanomaterials **11**(8), 1965 (2021)
24. Yun Chen, Cheng Zhang, Liyi Li, Chia-Chi. Tuan, Xin Chen, Jian Gao, Yunbo He, Ching-Ping. Wong, Effects of defects on the mechanical properties of kinked silicon nanowires. Nanoscale Res. Lett. **12**(1), 1–8 (2017)

25. S. K. Tippabhotla, W.J.R. Song, A. Subramani, C. V. Stan, N. Tamura, A. AO. Tay, A. S. Budiman (2019) Stress and fracture of crystalline silicon cells in solar photovoltaic modules–a synchrotron x-ray microdiffraction based investigation. MRS Advances, **4**(43), 2319–2335
26. Lara Ferrighi, Luca Frediani, Chiara Cappelli, Paweł Sałek, Hans Ågren, Trygve Helgaker, Kenneth Ruud, Density-functional-theory study of the electric-field-induced second harmonic generation (efishg) of push-pull phenylpolyenes in solution. Chem. Phys. Lett. **425**(4–6), 267–272 (2006)
27. Alex Masolin, Pierre-Olivier. Bouchard, Roberto Martini, Marc Bernacki, Thermo-mechanical and fracture properties in single-crystal silicon. J. Mater. Sci. **48**(3), 979–988 (2013)
28. M Mohammed, M. B. Khan, E. B. Mohammed Bashier (2016) Machine learning: algorithms and applications. Crc Press
29. C. Yang, Y. Kim, S. Ryu, G. X. Gu, Prediction of composite microstructure stress-strain curves using convolutional neural networks. Materials & Design, **189**, 108509 (2020)
30. Duyen H. Nguyen-Le, Q.B. Tao, Vu-Hieu Nguyen, Magd Abdel-Wahab, H. Nguyen-Xuan, A data-driven approach based on long short-term memory and hidden markov model for crack propagation prediction. Eng. Fracture Mech., **235**, 107085 (2020)
31. D. Samir Khatir, C.. Le. Boutchicha, H. Thanh, T.N. Tran-Ngoc, M. Abdel-Wahab. Nguyen, Improved ann technique combined with jaya algorithm for crack identification in plates using xiga and experimental analysis. Theo. Appl. Fracture Mech. **107**, 102554 (2020)
32. I. C. Gonnella, Martin W. Hess, G. Stabile, G. Rozza, A two stages deep learning architecture for model reduction of parametric time-dependent problems. arXiv e-prints, pages arXiv–2301, (2023)
33. B.A. Le, J. Yvonnet, Q.-C. He, Computational homogenization of nonlinear elastic materials using neural networks. Int. J. Numer. Methods Eng. **104**(12), 1061–1084 (2015)
34. S. Wang, H. Wang, Y. Zhou, J. Liu, P. Dai, X. Du, M. Abdel Wahab, Automatic laser profile recognition and fast tracking for structured light measurement using deep learning and template matching. Measurement **169**, 108362 (2021)
35. Somdatta Goswami, Cosmin Anitescu, Souvik Chakraborty, Timon Rabczuk, Transfer learning enhanced physics informed neural network for phase-field modeling of fracture. Theo. Appl. Fracture Mech. **106**, 102447 (2020)
36. Jianguo Yu, Susan B. Sinnott, Simon R. Phillpot, Charge optimized many-body potential for the si/ sio 2 system. Phys. Rev. B, **75**(8), 085311 (2007)
37. Tzu-Ray. Shan, Bryce D. Devine, Travis W. Kemper, Susan B. Sinnott, Simon R. Phillpot et al., Charge-optimized many-body potential for the hafnium/hafnium oxide system. Phys. Rev. B **81**(12), 125328 (2010)
38. J.J. Hopfield, Artificial neural networks. IEEE Circ. Devices Mag. **4**(5), 3–10 (1988)
39. Diederik P. Kingma, Jimmy Ba, Adam: A method for stochastic optimization. arXiv preprint arXiv:1412.6980, (2014)
40. Jason S. Schwarz, Chris Chapman, Elea McDonnell Feit, Welcome to python. In: Python for Marketing Research and Analytics, pages 3–7. Springer, (2020)
41. François Chollet et al, Keras: The python deep learning library. Astrophysics source code library, pages ascl–1806, (2018)